Dimethylamino group modified polydopamine nanoparticles with positive charges to scavenge cell-free DNA for rheumatoid arthritis therapy

Ying Chen [a,b,1], Yonglin Wang [a,c,1], Xianfang Jiang [a,d,1], Jinhong Cai [a,b], Yuting Chen [a,b,c], Hanji Huang [a,b], Yuan Yang [a,b,c,e], Li Zheng [a,b,e,*], Jinmin Zhao [a,b,c,e,**], Ming Gao [a,b,***]

[a] Guangxi Engineering Center in Biomedical Materials for Tissue and Organ Regeneration, The First Affiliated Hospital of Guangxi Medical University, Nanning, 530021, China

[b] Guangxi Collaborative Innovation Center of Regenerative Medicine and Medical Bioresource Development and Application, The First Affiliated Hospital of Guangxi Medical University, Nanning, 530021, China

[c] Department of Orthopedics, The First Affiliated Hospital of Guangxi Medical University, Nanning, 530021, China

[d] Department of Oral Radiology, College of Stomatology of Guangxi Medical University, Nanning, 530021, China

[e] Guangxi Key Laboratory of Regenerative Medicine, International Joint Laboratory on Regeneration of Bone and Soft Tissues, The First Affiliated Hospital of Guangxi Medical University, Nanning, 530021, China

ARTICLE INFO

ABSTRACT

Excessive cell-free DNA (cfDNA) released by damaged or apoptotic cells can cause inflammation, impacting the progression of rheumatoid arthritis (RA). cfDNA scavengers, such as cationic nanoparticles (NPs), have been demonstrated as an efficient strategy for treating RA. However, most scavengers are limited by unfavorable biocompatibility and poor scavenging efficacy. Herein, by exploiting the favorable biocompatibility, biodegradability and bioadhesion of polydopamine (P), we modified P with dimethylamino groups to form altered charged DPs to bind negatively charged cfDNA for RA therapy. Results showed that DPs endowed with superior binding affinity of cfDNA and little cytotoxicity, which effectively inhibited lipopolysaccharide (LPS) stimulated inflammation *in vitro*, resulting in the relief of joint swelling, synovial hyperplasia and cartilage destruction in RA rats. Significantly, DPs with higher DS of bis dimethylamino group exhibited higher positive charge density and stronger cfDNA binding affinity, leading to excellent RA therapeutic effect among all of the treated groups, which was even close to normal rats. These finding provides a novel strategy for the treatment of cfDNA-associated diseases.

1. Introduction

Cell-free DNA (cfDNA) is a DNA fragment that mainly derived from nuclear and mitochondrial of apoptosis or necrosis cell [1]. Increasing evidences suggested that cfDNA played an active role in inflammatory diseases. It also tightly participated in immune responses in physiological conditions and lead to sterile inflammation in pathological conditions [2,3]. Specifically, in rheumatoid arthritis (RA) patients, the levels

of cfDNA in synovial fluid (SF) and peripheral blood were highly elevated [4]. Genetic sequencing also identified that cfDNA in SF of RA was rich in hypomethylated cytosine-phosphate- guanosine (CpG) and could cause severe inflammation both *in vitro* and *in vivo* through upregulation of TNF-α expression [5,6]. Therefore, cfDNA is crucial for RA process.

Accumulating evidences indicated that cfDNA was one of the main reasons for RA occurrence [7–9]. CfDNA originated from mitochondrial

DNA, similar to bacterial DNA and would elicit high levels of oxidative damage. It could form complexes by binding with LL-37 [7], HMGB [10, 11], auto-Ig [12], or other proteins, leading to autoimmune response and driving the progression of variety inflammatory diseases [13]. Stimulation of TLR9 would also activate NF-kB, which consequentially resulted in the production of inflammatory factors like TNF-α and IL-6 [14,15]. Lack of DNase II also digested the chromosomal DNA from apoptotic cells so that mice with DNase II deletion developed a chronic polyarthritis similar to human RA. In these mice, TNF-α was upregulated in the bone marrow, and rheumatoid factors exhibited high levels in serum [16,17]. The above studies suggested that cfDNA could be a potential target for RA.

Scavenging cfDNA offers a new modality of treating RA. Although it was difficult to specifically clear cfDNA through the interaction of structural or complementary sequences [18], the anions of cfDNA were easy to be recognized by cationic polymers, which had been used as therapeutic targets recently [19]. Different charge density of nucleic acid-binding nanoparticles (NABNs) were used as cfDNA scavengers, whose binding affinity increased with their charge density. As a result, NABNs had strong attenuation capacity for cfDNA derived pro-inflammation *in vitro* and *in vivo* [20,21]. Cationic nanoparticles (NPs) could scavenge cfDNA from patients and further block the activation of primary fibroblast-like synoviocytes and SF monocytes. These cfDNA scavengers further relieved RA symptoms and achieved partial mobility recovery in a murine RA model [9,22]. Unfortunately, the above cationic NPs were limited by high cytotoxicity for further application.

Recently, polydopamine (PDA), a mussel-derived polymer, with minimal toxicity and favorable biodegradability has attracted tremendous attentions in biomedical application [23]. PDA and its derivatives also had potential scavenging effects on excessive reactive oxidative stress (ROS), further alleviating and treating ROS derived diseases such as ischemic stroke, Parkinson and osteoarthritis due to its abundant reductive groups like catechol and imine [24–27]. PDAs tended to target dopamine receptors, which were highly expressed in immune diseases including RA, and functions as immune system regulator as well [28]. Significantly, it had unique property of bioadhesion similar to

mussel-adhesive proteins that displayed high adhesion to most substrates [29]. PDA-based therapy had been confirmed as a favorable gene carrier, which could effectively adsorb DNA on the surface via polyvalent metal-mediated coordination [30,31]. Besides, PDA reacted towards amino or thiol groups via Schiff`s base reaction and Michael addition, which offered a simple way to modify the organic or inorganic materials. Thus, PDA NPs had been conjugated with polyethyleneimines (PEI) of different molecular weight (Mw) to form efficient gene transfection agents, which had abundant positive charges to efficiently bind with anionic plasmid DNA (pDNA) to form nanocomplexes with low cytotoxicity [32]. Furthermore, modified with PDA, a positively charged magnetic nanoparticle (PDA@Fe$_3$O$_4$) exhibited high adsorption capacity of DNA [33]. Therefore, PDA based nanocomposites with high positively charge density can act as excellent nanocarriers for gene binding.

In our study, to scavenge cfDNA in the treatment of RA, the positively charged DPs modified by 3- dimethylamino- 1- propylamine (M) or 3, 3- iminobis (N, *N*- dimethylaminopropyl) (B) were synthesized (Fig. 1). The abundant catechol and imine groups of P were firstly activated by 1, 1′- carbonyldiimidazole (CDI) followed by the reaction with amino groups of M or B to form dimethylamino group modified P (DP-M or DP-B) with varied charge density to bind negatively charged cfDNA. This novel cfDNA scavenger may exhibit strong binding affinity of cfDNA, inhibit the cfDNA induced inflammation with high efficiency, and consequently promote the RA therapeutic efficacy. The positively charged PDA NPs may provide a novel strategy for RA prevention and therapy.

2. Experimental section

2.1. Chemicals

3- hydroxytyramine hydrochloride (DA, ≥ 98%) was commercially obtained from Aladdin (China). Dimethyl sulfoxide (DMSO, ≥ 99.9%), 1, 1′- carbonyldiimidazole (CDI, ≥ 97.0%), 3- dimethylamino- 1- propylamine (M, ≥ 99%), 3, 3- iminobis (*N, N*- dimethylaminopropyl) (B, ≥ 97%) were purchased from Macklin (China). Ammonium hydroxide and
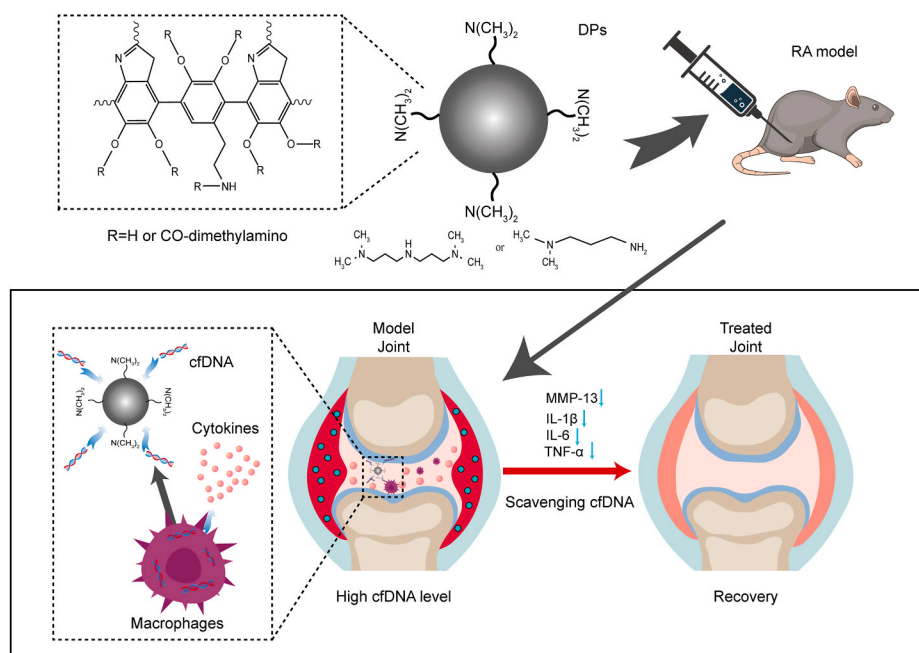
Fig. 1. Schematic illustration of *in vivo* RA therapy effect of dimethylamino group (3- dimethylamino- 1- propylamine (M) or 3, 3- iminobis (N, *N*- dimethylaminopropyl) (B)) modified polydopamine (DPs). The DPs were intra articular (IA) injected into the knee joint of CIA rat and strongly bound with cfDNA to lower the expression of inflammatory factors: MMP-13, TNF-α, IL-6 and IL-1β for RA therapy.

ethanol was obtained from Jinshan Chemical Reagent Co., Ltd (China) and Sinopharm Chemical Reagent Co., Ltd (China) respectively. All reagents were used directly without further purification.

2.2. Synthesis of PDA NPs

2.2.1. Preparation of P

P was synthesized according to previous literature [34,35], namely that DA polymerized via oxidation under an ethanol-alkaline aqueous solution. Firstly, ammonium hydroxide (3 mL), ethanol (40 mL), deionized (DI) water (90 mL) were mixed and DA (500 mg) was added into the solution with a dropwised manner. The mixture reacted for 24 h with stirring. Next, the solution was centrifuged for 10 min at 12000 rpm with a centrifuge (Eppendorf 5810R, Germany) and then washed with DI water for 3 times. Finally, the P was obtained by freeze-drying in a freeze dryer and stored at 4 °C.

2.2.2. Preparation of modified P

P (0.1 g) was added into dimethyl sulfoxide (DMSO, 20 mL, ≥ 99.9%) to obtain the mixed solution. And 0.2 g CDI was then added and stirred for 24 h. Next, to obtain four types of modified P, 0.5 or 1 mL of M and 0.55 or 1.1 mL B was separately added into the mixture before stirred for another 24 h. The reacted mixtures were centrifuged for 10 min at 12000 rpm and washed for 3 times with DI water. Finally, the modified P was obtained through freeze-drying, named as M modified P (DP-$M_{(L)}$ and DP-$M_{(H)}$) and B modified P (DP-$B_{(L)}$ and DP-$B_{(H)}$) respectively (Table S1).

2.3. Characterization of PDA NPs

These PDA NPs (including P, and DPs) were respectively characterized by using Fourier transform infrared spectrometer (FTIR, IRAffinity-1S, Shimadzu, Japan), Raman spectroscopy (JASCO NRS-4500, Japan), X-ray photoelectron spectroscopy (XPS, Thermo, UK) and X-ray diffraction (XRD, MiniFlex 600, Japan). And the morphology and distribution of these NPs were investigated by scanning electron microscope (SEM, Hitachi, Japan) coupled with energy dispersive X-ray spectroscopy (EDS), transmission electron microscopy (TEM, Hitachi, Japan) and atomic force microscopy (AFM, Bruker, US) respectively. The zeta potential of PDA NPs in PBS buffer was characterized by Nano-ZS (Malvern Panalytical, China) as well.

2.4. DNA binding capacity

The DNA binding capacity of P and DPs were detected by agarose gel electrophoresis, where CpG 1826 (TCCATGACGTTCCTGACGTT, GenScript, China) served as DNA. Details were: PDA NPs (100 μg) were added into CpG 1826 solution (1 μM in PBS, 2 mL) and incubated at room temperature (2 h). Then, the mixture (10 μL) was loaded on 2% agarose gel and the gel electrophoresis was implemented at 100 V for 40 min. Pure CpG 1826 was used as the control. And then the agarose gel was pre-stained with SuperRed/GelRed and imaged by Ultra-sensitive multifunctional imager (Amersham Imager 6000). Besides, the DNA ladder (50–1500 bp, Ameko Life sciences, China) was applied as the DNA template to investigate the binding ability of DPs. Briefly, DNA ladder (5 μL) was mixed with different PDA NPs (50 μg/mL, 10 μL) or DP-$B_{(H)}$ with different concentration (0, 10, 20, 50 and 100 μg/mL, 10 μL) for 2 h before implementing DNA gel electrophoresis (3% agarose gel, 100 V, 40 min). Furthermore, to confirm their DNA binding ability not affected by serum, the DNA ladder (5 μL) was initially mixed with 5 μL serum from SD rats for 10 min, and then respectively mixed with PDA NPs (50 μg/mL, 10 μL) for 2 h. Finally, the supernatant after centrifuge (500 ppm, 5 min) was collected for DNA gel electrophoresis (3% agarose gel, 100 V, 40 min).

2.5. Cytotoxicity assay of PDA NPs

2.5.1. Cell culture

RAW 264.7 cells were commercially purchased from American type culture collection (ATCC, USA). The chondrocytes were extracted from the knee joint of Sprague- Dawley (SD) rats (male, 3–5 day) and collected by centrifugation before cultured in Dulbecco modified eagle medium (DMEM, Gibco, USA) containing 10% (V/V) fetal bovine serum (FBS, Gibco, USA) and 1% penicillin/streptomycin (Solarbio, China). And the osteoblasts were extracted from the frontal and parietal bone of SD rats (male, 3–5 day). After cut into pieces, the bones were digested in trypsin (0.25%, Biosharp, China) at 37 °C for 10 min, and the precipitates were collected after centrifugation at 1000 rpm for 5 min and treated with collagenase II (Biofox, China) for further digestion. All cells were respectively cultured in Dulbecco modified Eagle medium. The cultured medium was replaced every 2 days. Cells were passaged when reaching 85%–90% and collected for further research.

2.5.2. Cell counting kit- 8 testing

The cell cytotoxicity of PDA NPs was evaluated by cell counting kit- 8 (CCK- 8, Dojindo, Japan) assay, implemented as following: RAW264.7, chondrocytes and osteoblast were respectively seeded in 96- well plates with the density of 5000 cells per well. And the cultured medium was replaced with fresh medium containing DPs with different concentrations (0, 5, 10, 20, 50, 100 and 200 μg/mL). After incubation (24 h), the cells were washed for 3 times with PBS buffer and incubated in 100 μL medium (10% CCK-8). The absorbance was recorded at 450 nm by spectrophotometer (Thermo Fisher, USA). And the viability of cells was calculated by comparing with control group (only fresh medium) and the experiment was repeated in triplicates.

2.5.3. Live/dead staining assay

To establish the inflammatory cell model, RAW264.7 cells (15×10^4 cells/mL) were stimulated with lipopolysaccharide (1 μg/mL) (LPS, Solarbio, China) following previously reported work, which also confirmed that LPS stimulation could increase the amount of cfDNA [36]. After 24 h' incubation, the stimulated cells were further co-cultured with 50 μg/mL PDA NPs for another 24 h. Finally, the treated cells were used for further researches including live/dead staining, qRT-PCR and immunofluorescent staining. The live/dead staining was implemented using a Calcein- AM/PI assay kit (Sigma, USA). Briefly, PDA NPs treated RAW264.7 cells were incubated with calcein and propidium iodide (PI) for 5 min in the darkness. After PBS buffer washing, the cells were imaged by microscope (Olympus BX53, Tokyo, Japan).

2.6. Quantitative real-time polymerase chain reaction (qRT-PCR) and enzyme linked immunosorbent assay (ELISA)

The gene expression levels of inflammatory factor including TNF-α, IL-1β, iNOS and IL-6 were separately quantified by qRT-PCR. Total RNA of RAW264.7 cells was isolated by RNA extraction kit (Magen, China) following the protocol. The qRT-PCR reaction was conducted by the LightCycler® System (Roche, Switzerland). All primer sequences of these genes were presented in Table S2. The levels of relative gene expression were analyzed by the $2^{-\Delta\Delta CT}$ method and normalized with glyceraldehyde- 3- phosphate dehydrogenase (GAPDH). Besides, the supernatant of LPS induced RAW264.7 was collected to investigate the expression of inflammatory factors (IL-6 and TNF-α) by ELISA kit following the instruction of manufacturer [37,38].

2.7. Immunofluorescence

To further verify the change of inflammatory factors of RAW264.7 cells after treated with PDA NPs, the protein expression of iNOS, TNF-α and MMP-13 was identified by immunofluorescent staining. At the

beginning, the cells were firstly fixed with paraformaldehyde solution (4%, Biosharp, China) for 10 min. After being treated with 3% H_2O_2 for 15 min, the cells were blocked with goat serum to avoid nonspecific binding and incubated with primary antibody of iNOS, TNF-α or MMP-13 (1: 200 dilution) (Boster, China) separately overnight at 4 °C. And then, the cells were added with FITC- anti-rabbit IgG (Boster, China) for incubation (1 h) in the dark before the nuclei was stained with DAPI (5 min). The pictures were finally imaged by fluorescence microscope (Olympus, Japan).

2.8. Cellular colocalization of Cy5-CpG 1826 and PDA NPs

RAW264.7 cells were initially cultured in 6- well plate with the density of 15×10^4 cells per well. Then, 2 μL Cy5-CpG 1826 (Cy5-TCCATGACGTTCCTGACGTT, 1 μM, GenScript, China) was added into the cultured medium and incubated for another 4 h [39,40]. The excessive Cy5-CpG 1826 was removed by washing with PBS for 3 times before the addition of FITC labeled PDA NPs (50 μg/mL) or not. After incubation (24 h), the cells were stained with Lyso- Tracker Red (Beyotime, China) and DAPI for observation by confocal microscope (Leica SP8, Germany). The mean fluorescent intensity of Cy5-CpG 1826 was analyzed by Image J. And the colocalization ratio of Cy5-CpG 1826 and FITC-PDA NPs was calculated by the ratio of colocalization area (white) and foreground area (green and purple).

2.9. In vivo degradation of PDA NPs

The in vivo imaging systems (IVIS, Lumina LT, US) were applied to evaluate the *in vivo* retention and biodistribution of PDA NPs [41]. At the beginning, 20 mg DP-B$_{(H)}$ were dispersed in 100 μL DMSO with stirring. Later, 20 μL cyanine 5 NHS ester (Cy5, 50 mg/mL, Lumiprobe) was added into the solution followed by the addition of triethylamine (50 μL). The mixture reacted for 24 h before centrifugation and washing with ethanol for 3 times. After vacuum drying, the sample (Cy5-DP-B$_{(H)}$) was isolated for further experiment. For *in vivo* degradation, Cy5-DP-B$_{(H)}$ (50 μg/mL, 20 μL) was intra-articular (IA) injected into SD rat (180–200 g). The images were taken at predetermined time points (0, 4, 8, 24, 48, 72, 96 and 120 h) with the excitation and emission wavelength at 646 nm and 662 nm. After 120 h, the major organs including heart, liver, spleen, lung and kidney from SD rats were taken out for IVIS imaging as well.

2.10. RA model establishment and in vivo experiment

Five ∼ six weeks' female SD rats (180–200 g) were chosen to implement the experiment *in vivo*. The *in vivo* studies were approved by the Animal Ethics Committee of Guangxi Medical University with the Guide of Care and Use of Laboratory Animals. The rheumatoid arthritis animal (CIA) model was established by tail injection of type II collagen (Col2) solutions (initial immunization: 50 μL Col2 and 50 μL complete Freund adjuvant (CFA, 2 mg/mL), and booster immunization: 50 μL Col2 and 50 μL Freund incomplete adjuvant (FIA) after one week, totally 100 μL per SD rat for every immunization) according to previous work [42]. At the 13th day, RA rats were randomly divided into four groups: RA (only PBS buffer injection), P (P injection), DP-M$_{(H)}$ (DP-M$_{(H)}$ injection), and DP-B$_{(H)}$ (DP-B$_{(H)}$ injection). All NPs were IA injected into knee joints with a dose of 2.5 mg/kg every 3 day (totally 4 times till sacrificed). SD rats without any treatments were used as normal group.

2.11. In vivo evaluation of RA therapy

2.11.1. Joint swelling evaluation
The swelling degree of joints was evaluated every 3–4 day (day 14, 17, 21, 24 and 27) from the onset of RA (day 13) until the rats were killed. The swelling of joints was evaluated based on the diameter of rats' ankle with vernier caliper (Guanglu, China). And the clinical scores

of hind paw of each rats were calculated according to the previous evaluation method [43], where score 0, 1, 2, 3 and 4 corresponded to no swelling, mild swelling, mild swelling, moderate swelling and severe swelling respectively.

2.11.2. Inflammatory factors measurement
The expression levels of inflammatory factors in serum and SF were investigated to evaluate the treatment effect. The whole blood was collected from all rats and treated with heparin for anticoagulation before being centrifuged at 1500 rpm for 10 min. After the plasma was separated, the inflammatory factors (IL-6, MMP-13, TNF-α and IL-1β) of serum were measured using the commercially available ELISA kit (Meimian, China) by the instruction of manufacturer. The absorbance at 450 nm was recorded by the microplate reader. Similarly, the SF was collected from articular cavity after injecting 50 μL PBS buffer and further measured the expression of inflammatory factors (IL-6, MMP-13 and TNF-α) by ELISA.

2.11.3. Histological evaluation
Rats were sacrificed after treated with PDA NPs for 2 weeks. The ankles and knees were fixed with paraformaldehyde (4%) for 2 days. Then, all samples were incubated in 10% ethylenediaminetetraacetic acid (EDTA, Solarbio, China) buffer solution for decalcification using Ultrasonic Decalcifying Unit (USE 33, Medite, Germany) for 4 weeks. Later, the tissues were embedded in paraffin and sliced into 5 μm thickness of tissue sections. The slides were finally stained with Hematoxylin-eosin (HE, Solarbio, China) or Safranin- O fast green (Solarbio, China) before the images were obtained using a microscope (Olympus BX53, Japan).

The immunohistochemical staining was applied to identify the expression of IL-6, MMP-13 and TNF-α in the cartilage. In brief, the knee tissue sections were incubated with 3% H_2O_2 for 10 min before blocked by goat serum for 30 min. Subsequently, tissue sections were separately incubated with primary antibody of TNF-α, MMP-13 or IL-6 (1: 200 dilution, Boster, China) for 60 min with humidified chamber (37 °C). After PBS buffer washing for 3 times, the sections were incubated with secondary antibody (biotin-labeled goat anti-mouse/rabbit IgG (ZSGb Bio, China)) for another 30 min. Later, samples were stained with 3, 3′-diaminobenzidine tetrahydrochloride (DAB, Boster, China) before counterstained with hematoxylin (Solarbio, China). The sections were finally sealed with neutral resin before imaging (Olympus BX53, Tokyo, Japan).

2.11.4. Other markers' evaluation
The bone damage of knee joints was investigated by using ex-vivo micro-computed tomography (μCT-100, Swiss, SCANCO Medical AG) and scanned with the resolution of 15 μm (70 kV and 200 μA) after fixation (4% paraformaldehyde). Then, the dataset was reconstructed to obtain 3D images of joints and the bone mineral density (BMD) was also measured using Inveon Research Workplace. And the body weight of each rats was weighed by animal weight balance (Shanghai Yu yan, China) during the RA therapy. Meanwhile, the cfDNA was extracted from peripheral blood sample of rats based on cfDNA extraction kit (Ezup, Sangon Biotech, Shanghai) by following the manufacture's instruction. Furthermore, the major organs including heart, liver, spleen, lung and kidney were fixed with 4% paraformaldehyde and cut into 2 μm thickness after H&E staining for histological evaluation.

2.12. Statistical analysis

All experiments were carried out at least in triplicates. And the data were analyzed by SPSS 20.0 (SPSS Inc., Chicago, Illinois, USA) and presented as mean ± standard deviation. The differences between two groups were analyzed with one-way ANOVA followed by Game Howell analysis or Least Significant Difference (LSD) analysis.

3. Results and discussion

3.1. Preparation and characterization of PDA NPs

P was prepared through polymerization of DA under alkaline conditions via oxidative self-polymerization. Next, four types of dimethylamino group modified P (DPs), referred to as DP-M$_{(L)}$, DP-M$_{(H)}$, DP-B$_{(L)}$, and DP-B$_{(H)}$ were successfully fabricated via modification with different concentrations of M or B (Fig. 2A). Table S3 illustrated the recipe of preparation of DPs. After calculation, the degree of substitution (DS) was 1.2% and 7.6% for DP-M$_{(L)}$ and DP-M$_{(H)}$ with M modification, and 1.8% and 7.5% for DP-B$_{(L)}$ and DP-B$_{(H)}$ with B modification respectively. In Fig. 2B, it displayed the zeta potential of PDA NPs before and after modification. The zeta potential of P was −21.76 mV, which respectively increased to −14.36 and + 1.35 mV for DP-M$_{(L)}$ and DP-M$_{(H)}$ after M modification. Similarly, the zeta potential was −12.86 mV for DP-B$_{(L)}$ and it increased to +10.33 mV for DP-B$_{(H)}$. After interacted with M or B, the introduction of positively charged dimethylamino groups significantly improved the positive charge density of P. Significantly, high DS of bis dimethylamino groups (DP-B$_{(H)}$) contributed to high positive charge density compared to DP-B$_{(L)}$ with low DS of bis dimethylamino groups and DP-M$_{(H)}$ with the same high DS of mono dimethylamino groups.

Meanwhile, FTIR was performed to characterize PDA NPs (Fig. 2C). The wavelength bands observed at 3350–3450 cm^{-1} corresponded to the ν (O–H) and ν (N–H) functions, which represented the phenolic hydroxyl and amino groups of P. And the characteristic bands of P were also obviously observed for all modified P due to the introduction of amine groups (N–H and N–C). On the other hand, the peak at 1708 cm^{-1} (C=O) was observed for DP-M$_{(L)}$, DP-M$_{(H)}$, DP-B$_{(L)}$ and DP-B$_{(H)}$ originated from CDI activation during the reaction, indicating the successful modification of M or B. Besides, PDA NPs was also investigated by XPS. As illustrated in Figs. S1 and C, N, O elements were obviously observed for P and DPs. For detailed C1s, N1s and O1s spectrum, no significant difference existed for P before and after modification (Fig. S2).

The crystal structure of PDA NPs was characterized by XRD (Fig. 2D). As indicated in XRD patterns, a narrow and strong peak was observed at 2θ = 22.9°, caused by the existence of amorphous carbon of biochar containing the aromatic carbon sheets, also a characteristic peak of P. No significant differences were observed for XRD patterns of all NPs even after modification.

The molecular structure of PDA NPs was also tested by Raman spectroscopy. From Fig. S3, the apparent Raman shift (1000–1750 cm^{-1}) was observed for P while the Raman shift became weak after modification. Significantly, the new shift existed at 250–750 cm^{-1} for DPs, more obvious observed with the increase of DS of dimethylamino groups.

The morphology of PDA NPs was observed by TEM and AFM. As indicated in Fig. 2E, P and DPs remained the spherical shape with a size of 120–160 nm. Besides, the height of all PDA NPs was around 100 nm by AFM (Fig. 2F). In addition, PDA NPs was also investigated by SEM-EDS. As shown in Fig. S4, PDA NPs maintained the spherical shape even
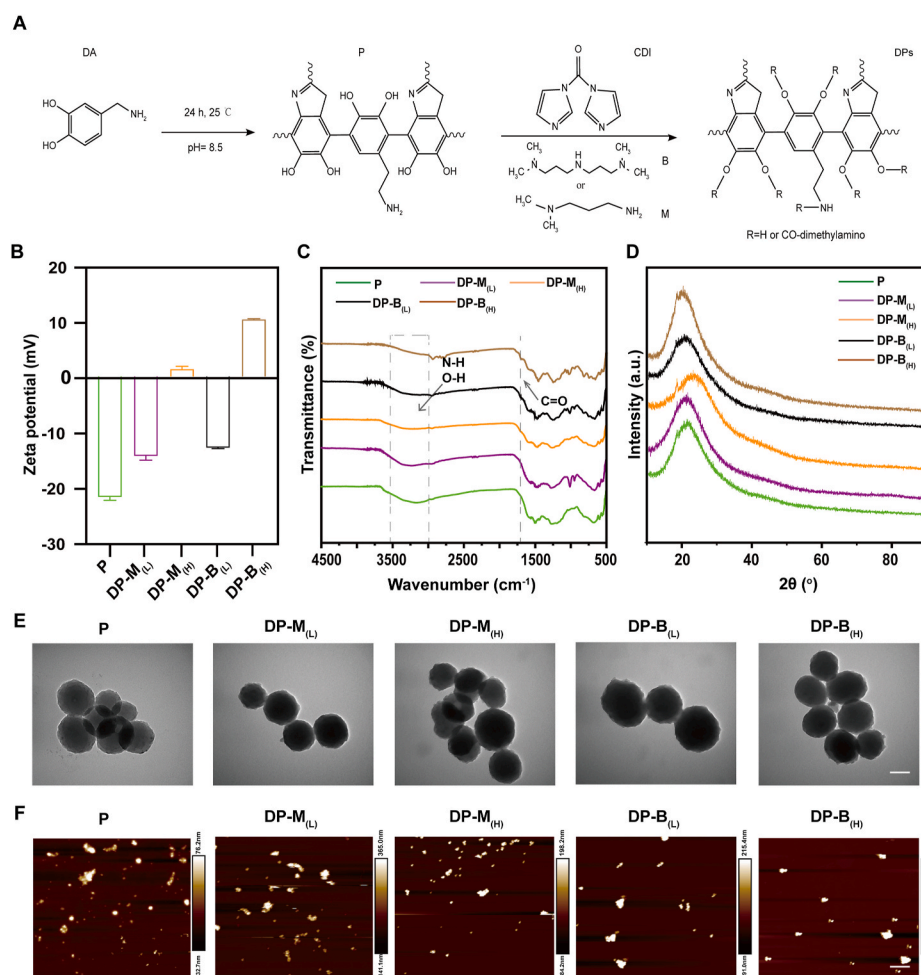
Fig. 2. Synthesis and physicochemical characterization of PDA NPs: P and dimethylamino groups modified P (DPs): DP-M$_{(L)}$, DP-M$_{(H)}$, DP-B$_{(L)}$ and DP-B$_{(H)}$. A) The synthesis routes of DPs via the activation of P by CDI followed by the reaction with M or B. B) Zeta potential of PDA NPs. C) FTIR results of PDA NPs. D) XRD results of PDA NPs. E) TEM results of PDA NPs. (Bar = 100 nm) F) AFM results of PDA NPs. (Bar = 4 μm).

after modification. And PDA NPs still kept the same element composition: C, N and O.

From the above, it confirmed that the morphology, molecular composition and crystal structure of DPs was similar to the pure P, indicating that the introduction of dimethylamino groups did not affect the structural characteristics of PDA NPs but only contribute to the adjustment of positive charge density.

3.2. Cytotoxicity of PDA NPs

The cytotoxicity on RAW 264.7, chondrocytes and osteoblasts were detected through CCK- 8 assay. As shown in i of Fig. 3A, within the concentration range of 0–50 μg/mL, the cytotoxicity of all NPs was minimum with the cell viability above 95%. However, when the concentration was above 100 μg/mL, the cell viability of DPs started to decrease, indicating that cells would suffer a certain of cytotoxicity. But the viability was still above 60%, attributed to the enrichment of positive charges. Similarly, the chondrocytes displayed the same tendency of cell viability, with a little cytotoxicity at 200 μg/mL (ii of Fig. 3A). However, as indicated in iii of Fig. 3C, almost no cytotoxicity existed for osteoblasts, with the cell viability above 95% during the concentration ranges from 0 to 200 μg/mL. Yan et al. [13] had also found that although higher positive charge of cationic cfDNA scavengers could be conducive to DNA binding efficiency and showed longer retention time in psoriatic lesions, improving therapeutic outcome, it also increased cell cytotoxicity at the same time. Therefore, 50 μg/mL was chosen for subsequent experiments.

Additionally, the live/dead staining was also applied to investigate the protection capacity of PDA NPs. Compared to normal group, the quantity of live cells obviously decreased and a lot of dead cells were observed for control group (LPS induced cells) with the live/dead ratio of 8.6%. However, the quantity of live cells increased and the number of dead cell decreased after PDA NPs (50 μg/mL) treatment so that the live/dead ratio was above 80% for all other groups (Fig. 3B and C). It suggested that PDA NPs exhibited almost no cytotoxicity and also had the protection capacity of LPS induced cells by preventing inflammation if the concentration was below 100 μg/mL.

3.3. Anti-inflammatory capacity in vitro

The anti-inflammatory capacity of PDA NPs was evaluated by qRT-

PCR via the inflammatory factors' expression levels. As illustrated in Fig. 4A, LPS stimulation remarkably increased the expression of iNOS, TNF-α, IL-1β and IL-6, slightly decreased by P treatment. It had already demonstrated that P could lower the expression of inflammatory factors. However, modified P displayed noticeable inhibition effects on LPS induced inflammation, especially for DP-B$_{(H)}$ with the lowest expression of inflammatory factors among the groups, such as iNOS and TNF-α almost close to normal group. After calculation, the expression of iNOS, TNF-α, IL-1β and IL6 decreased significantly by 63.9%, 34.1%, 59.6% and 70.4% respectively for DP-B$_{(H)}$ compared to control group. Meanwhile, the inflammatory factors expression of supernatant from LPS stimulated cells was also evaluated by ELISA. As shown in Fig. S5, LPS stimulation obviously increased the expression of IL-6 (A) and TNF-α (B) compared to normal macrophages. Pure P could slightly decrease the expression of IL-6 and TNF-α while DPs significantly lower their expressions. Among the DPs, DP-B$_{(H)}$ with high DS of bis dimethylamino group presented the lowest expression of both inflammatory factors, close to normal macrophages.

Besides, the immunofluorescence staining of inflammatory factors: iNOS, TNF-α and MMP-13 was also illustrated in Fig. 4B. For normal group, no fluorescent intensity was observed while the fluorescent intensity significantly increased after LPS stimulation. Especially, the fluorescent intensity of inflammatory factors decreased in P and DPs. In accordance with the results of qRT-PCR, DP-B$_{(H)}$ manifested quite evident anti-inflammatory effects than the other NPs with the significantly decreased expression of iNOS, TNF-α and MMP-13. After statistical analysis, the iNOS expression was 49% after LPS stimulation and it decreased to 38% for P and below 26% for DPs, which presented the same tendency as the expression of TNF-α and MMP-13. Among the modified P, the tendency for lowering the inflammatory factors was DP-M$_{(L)}$< DP-B$_{(L)}$< DP-M$_{(H)}$< DP-B$_{(H)}$. Significantly, the expression of TNF-α and MMP-13 was 8% and 7% for DP-B$_{(H)}$, infinitely close to normal group. As P itself displayed partly influence on the release of inflammatory factors from macrophages, the enhanced anti-inflammatory capacity of DPs attributed to the rise of charge density, especially when the charge was converted from negative to positive, which facilitated the cfDNA binding and scavenging [44]. In the meantime, DP-B$_{(H)}$ with the high DS of bis dimethylamino group performed the strongest binding affinity of cfDNA, further most effectively reducing the expression of inflammatory factors.
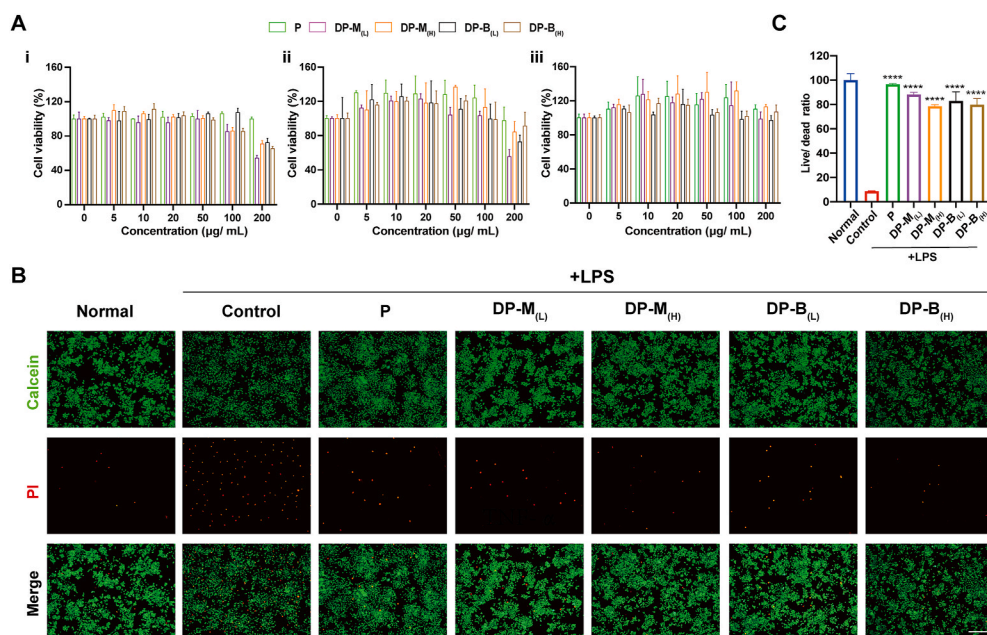
Fig. 3. Cell viability and protective effect of PDA NPs. A) Cell cytotoxicity of PDA NPs by CCK- 8 assay: macrophages (i), chondrocytes (ii) and osteoblasts (iii). B) Live/dead staining of LPS treated macrophages (100 μM, 4 h) followed by incubation with PDA NPs (50 μg/mL) for 24 h by fluorescence microscope. C) Quantified results of live/dead staining of LPS treated macrophages. The corresponding groups respectively were: normal (normal macrophages), control (LPS treated macrophages), LPS + P (LPS treated macrophages followed by P incubation), LPS + DP-M$_{(L)}$ (LPS treated macrophages followed by DP-M$_{(L)}$ incubation), LPS + DP-M$_{(H)}$ (LPS treated macrophages followed by DP-M$_{(H)}$ incubation), LPS + DP-B$_{(L)}$ (LPS treated macrophages followed by DP-B$_{(L)}$ incubation), LPS + DP-B$_{(H)}$ (LPS treated macrophages followed by DP-B$_{(H)}$ incubation). (Bar = 100 μm) ("*" symbol compared with the control group, ****p < 0.0001).
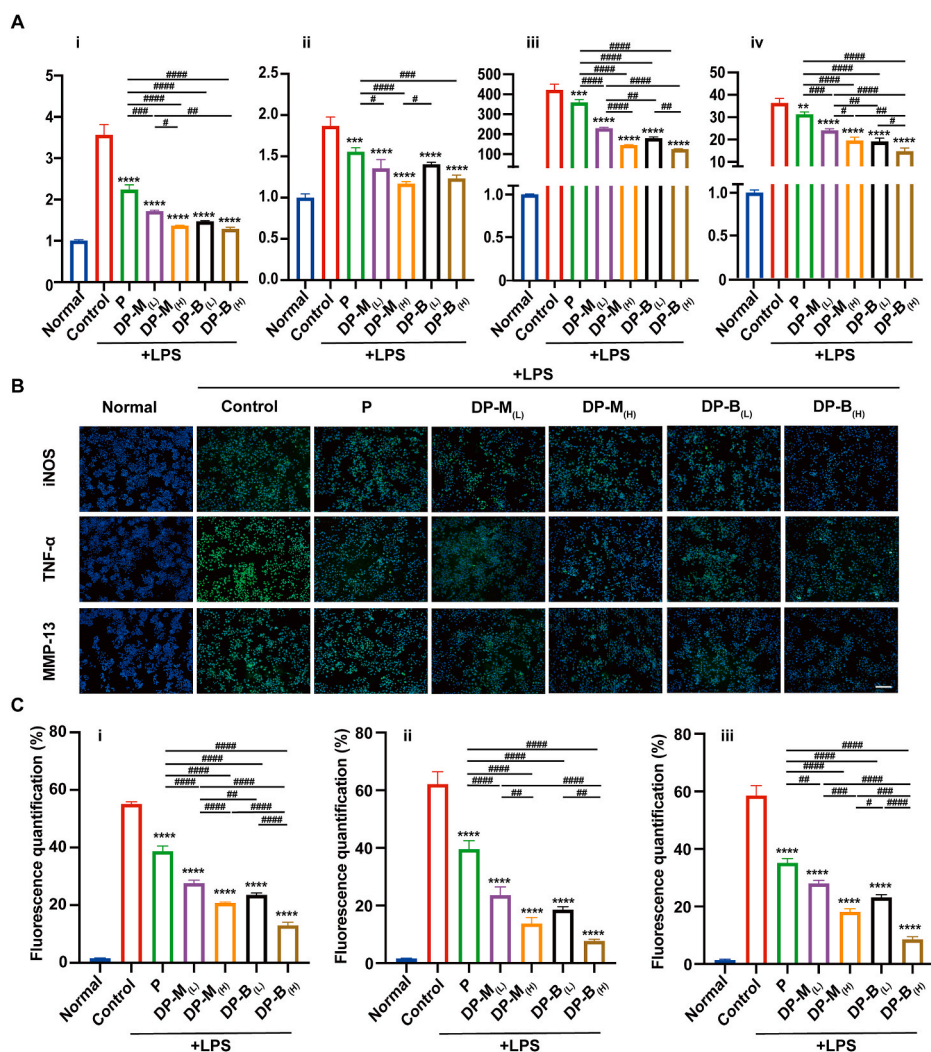
Fig. 4. *In vitro* anti-inflammatory capacity of PDA NPs. A) Gene expression of inflammatory factors: iNOS (i), TNF-α (ii), IL-6 (iii) and IL-1β (iv) by qRT-PCR. B) Inflammatory factors expression of LPS treated macrophages (100 μM, 4 h) followed by incubation with PDA NPs (50 μg/mL) for 24 h by fluorescence microscope and the corresponding quantified results of iNOS (i), TNF-α (ii), MMP-13 (iii) (C). The corresponding groups respectively were: normal (normal macrophages), control (LPS treated macrophages), LPS + P (LPS treated macrophages followed by P incubation), LPS + DP-M$_{(L)}$ (LPS treated macrophages followed by DP-M$_{(L)}$ incubation), LPS + DP-M$_{(H)}$ (LPS treated macrophages followed by DP-M$_{(H)}$ incubation), LPS + DP-B$_{(L)}$ (LPS treated macrophages followed by DP-B$_{(L)}$ incubation), LPS + DP-B$_{(H)}$ (LPS treated macrophages followed by DP-B$_{(H)}$ incubation). (Bar = 100 μm) ("*" symbol compared with control group, **p < 0.01, ***p < 0.001 and ****p < 0.0001, and "#" symbol compared between groups, #p < 0.05, ##p < 0.01, ###p < 0.001 and ####p < 0.0001).

3.4. DNA binding affinity in vitro

DNA binding affinity of PDA NPs was initially evaluated through agarose gel electrophoresis. As shown in Fig. 5A, the bands of P were similar to that of free CpG 1826, which indicated that there was no loss of DNA after P treatment and almost no DNA binding affinity of P. However, the bands became weak for DPs with different DS, especially for DP-M$_{(H)}$ and DP-B$_{(H)}$, suggesting that positively charged PDA NPs could effectively interact with negatively charged DNA and prevented the migration of DNA during gel electrophoresis. After statistic calculation, for 2 nmol CpG, the binding capacity of 100 μg P was 12.99% while it became 42.32%, 94.22%, 37.05% and 97.63% for DP-M$_{(L)}$, DP-B$_{(L)}$, DP-M$_{(H)}$ and DP-B$_{(H)}$ successively (Fig. 5B). Meanwhile, DNA ladder (50–1500 bp) was also applied as the DNA template to investigate the DNA binding ability. P had no binding ability of DNA with the DNA bands close to the DNA ladder. However, the bands from (50–250 bp) obviously disappeared for DP-M$_{(H)}$ while most of bands disappeared in the whole range with the same amount (Fig. S6A). As shown in Fig. S6B, the bands became lighter with the increase of DP-B$_{(H)}$ amount. When the concentration was 100 μg/mL, all bands disappeared. High DS of bis dimethylamino group was helpful to high DNA binding ability. Besides, it was expected that DNA binding ability still maintained efficient even in the serum condition. Compared to DNA ladder without treatment, the bands of DNA ladder changed a little after P incubation in the existence of serum, with darker bands observed at 550–600 bp. However, DPs obviously decreased the intensity of bands. Especially, the lighter bands

(around 50–200 bp) was apparently observed for DP-M$_{(H)}$ and DP-B$_{(H)}$ (Fig. S7). The positively charged DPs possessed strong DNA binding ability, even in the existence of serum. And the binding ability was enhanced with the increase of positive charge density, contributed by the high DS of bis dimethylamino groups.

Furthermore, the DNA binding affinity was also investigated by colocalization immunostaining of CpG 1826 and PDA NPs. CpG 1826 and PDA NPs were labeled with Cy5 (purple) and FITC (green) respectively. In Fig. 5C, it displayed that P was dispersed in the nucleus, lysosome and cytoplasm but not binding to CpG 1826, whereas no colocalization area (white area) was observed. However, the white area was observed for DP-M$_{(L)}$ and DP-B$_{(L)}$. Most significantly, there were much more white areas for DP-M$_{(H)}$ and DP-B$_{(H)}$. The overlay intensity of Cy5 and FITC, corresponding to the colocalization of CpG 1826 and PDA NPs, was illustrated in Fig. 5D. After statistical analysis, the ratio of cellular uptake was 58% for DP-B$_{(H)}$ and 43% for DP-M$_{(H)}$, almost twice more than that of DP-B$_{(L)}$ (31%) and DP-M$_{(L)}$ (22%) while it was only 3% for P, indicating that the modified P could efficiently bind DNA and high positive charge density always contributed to strong binding affinity. The above results also demonstrated that the positively charged DPs exhibited favorable DNA binding affinity.

3.5. In vivo degradation

The *in vivo* degradation of PDA NPs was evaluated by IVIS imaging. For unmodified DP-B$_{(H)}$, almost no fluorescent intensity was observed
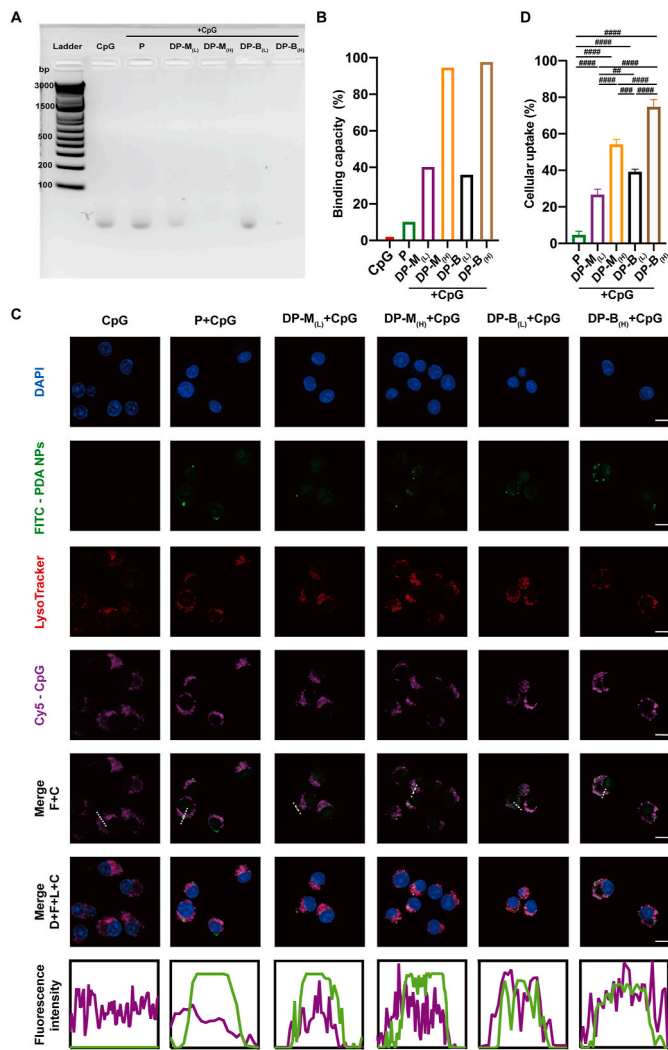
Fig. 5. The inhibition of intracellular CpG 1826 by PDA NPs. A) DNA binding capacity of PDA NPs by agarose gel electrophoresis (the corresponding bands successively were: DNA ladder, CpG alone, CpG + P, CpG + DP-M$_{(L)}$, CpG + DP-M$_{(H)}$, CpG + DP-B$_{(L)}$ and CpG + DP-B$_{(H)}$) and the corresponding quantified results (B). C) Immunofluorescent images of intracellular localization of CpG and PDA NPs in RAW264.7 cells after 8 h' incubation and the colocalization of fluorescent intensity of CpG (purple) and PDA NPs (green). (D, F, L and C indicated DAPI, FITC, LysoTracker and Cy5-CpG respectively) D) Quantified results of intracellular CpG colocalization. The corresponding groups respectively were: CpG (CpG treated macrophages), CpG + P (CpG treated macrophages followed by P incubation), CpG + DP-M$_{(L)}$ (CpG treated macrophages followed by DP-M$_{(L)}$ incubation), CpG + DP-M$_{(H)}$ (CpG treated macrophages followed by DP-M$_{(H)}$ incubation), CpG + DP-B$_{(L)}$ (CpG treated macrophages followed by DP-B$_{(L)}$ incubation), CpG + DP-B$_{(H)}$ (CpG treated macrophages followed by DP-B$_{(H)}$ incubation). (Bar = 100 μm) ("#" symbol compared between groups, ##$p < 0.01$, ###$p < 0.001$ and ####$p < 0.0001$). (For interpretation of the references to colour in this figure legend, the reader is referred to the Web version of this article.)

from the beginning to the end. Slightly intensity appeared in the ankle joint due to the noise of IVIS (Fig. S8A). However, as illustrated in Fig. S8B, the fluorescent intensity was obviously observed in the right knee joint of SD rat after Cy5-DP-B$_{(H)}$ injection. The fluorescent intensity gradually decreased versus time. After 120 h, the fluorescent intensity almost disappeared. Similarly, no fluorescent intensity existed in other major organs except for some noise observed in left knee or ankle joints. Besides, the major organs of rats were also taken out for IVIS. No fluorescent intensity was observed for all organs, indicating no cytotoxicity for organs (Fig. S9). From the above, PDA NPs presented a certain of

retention time inside the articular cavity and gradually degraded versus time *in vivo*. Therefore, PDA NPs possessed favorable biocompatibility and showed great potentials in clinic application.

3.6. RA therapy in CIA rats

As DP could effectively bind to cfDNA and further inhibit the LPS stimulated inflammation of RAW 264.7 cells, the therapeutic effects in CIA model were evaluated through analysis of the remission of symptoms and protection of damaged cartilage and bone. Fig. 6A illustrated
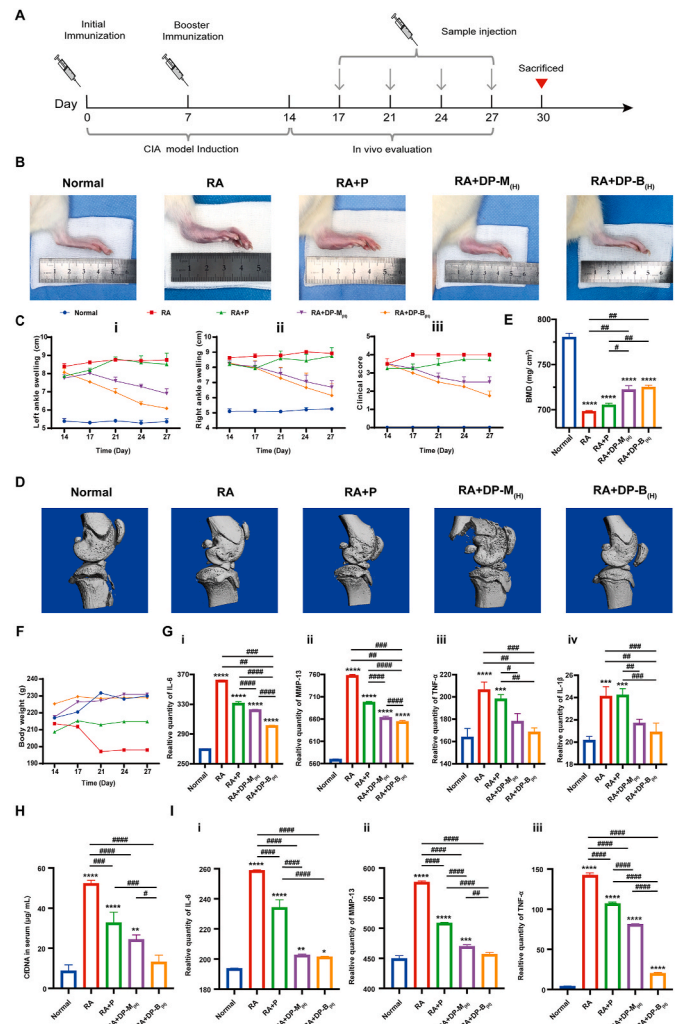
Fig. 6. *In vivo* RA therapy effects. A) Experimental schedule of the establishment of CIA model followed by the design of RA therapy. B) Side views of hindpaw swelling thickness of CIA rats after PDA NPs therapy. C) Average hindpaw swelling thickness determined every 3–4 day using a vernier caliper: left ankle (i), right ankle (ii) and the clinical score (iii) of hindpaw in CIA rats. D) Representative μCT 3D reconstructed images of knee joints of CIA rats after PDA NPs therapy (with the resolution of 15 μm) and the corresponding bone mineral density (BMD) (E). F) The body weight changes of CIA rats during the progression of RA therapy. G) The expression of inflammatory factors: IL-6 (i), MMP-13 (ii), TNF-α (iii) and IL-1β (iv) for serum by ELISA. H) The concentration of cfDNA in serum after PDA NPs therapy at day 30. I) The expression of inflammatory factors: IL-6 (i), MMP-13 (ii) and TNF-α (iii) for SF by ELISA. The corresponding groups respectively were: normal (normal rats), RA (CIA rats), RA + P (CIA rats followed by P treatment), RA + DP-M$_{(H)}$ (CIA rats followed by DP-M$_{(H)}$ treatment), RA + DP-B$_{(H)}$ (CIA rats followed by DP-B$_{(H)}$ treatment). ("*" symbol compared with RA group, **$p < 0.01$, ***$p < 0.001$ and ****$p < 0.0001$, and "#" symbol compared between groups, #$p < 0.05$, ##$p < 0.01$, ###$p < 0.001$ and ####$p < 0.0001$).

the establishment of CIA model and experimental schedule of RA therapy. As known to all, the clinical findings of RA affected joints were painful and swollen joints due to the high levels of inflammatory cytokines and accumulation of excessive SF [45]. Under microscope, RA was characterized by synovial inflammation and hyperplasia with pannus formation, causing bone and cartilage destruction [46]. In synovial tissues, lymphocytes and synoviocytes produced excessive inflammatory cytokines, such as IL-6, IL-1β and TNF-α, leading to synovitis [47]. Furthermore, cytokine stimulated synoviocytes secreted MMP and receptor activator of nuclear factor kappa B ligand (RANKL) into SF and consequently lead to cartilage degradation and joint destruction [48]. The pathobiology progression of CIA rat model was similar to that in RA patients. Not surprisingly, in Fig. 6B, CIA rats was accompanied by swelling and erythema in ankle and claw joints (RA group) compared to normal rats (Normal group). Meanwhile, the swelling thickness and erythema had not improved for RA + P group while the joints of RA + DP-M$_{(H)}$ and RA + DP-B$_{(H)}$ groups had obviously repaired. After quantification, the thickness of swelling maintained relatively stable around 8.7–8.9 cm for both ankles of RA group, much larger than those of normal group (around 5.1–5.8 cm). And the swelling thickness of RA + P group presented almost the same level as that of RA group, indicating that pure P had no effects on RA therapy. However, the swelling thickness of both ankles significantly decreased during the progression of DP-M$_{(H)}$ and DP-B$_{(H)}$ treatment. Significantly, the therapeutic effects of DP-B$_{(H)}$ were better than that of DP-M$_{(H)}$, where the thickness of both ankles was from 8.3-8.4 cm to 7.2–7.4 cm during the therapy process for DP-M$_{(H)}$ while it was 8.3–8.4 cm at the beginning and 6.2–6.3 at day 27 for DP-B$_{(H)}$ (i and ii of Fig. 6C). From iii of Fig. 6C, it displayed the clinical scores of swelling thicknesses after therapy. DP-B$_{(H)}$ and DP-M$_{(H)}$ had the obvious therapeutic effects with the clinical score of 2.3 and 1.7 at day 27 while it was 4.0 and 3.9 for RA and RA + P groups respectively.

Besides, the images of μCT were illustrated in Fig. 6D. The smooth surface of joint was observed for normal group where the joint surface became rough for RA group. However, the joint surface became relatively smooth after PDA NPs treatment. And the BMD was analyzed from μCT results. As shown in Fig. 6E, the BMD was 780 mg/cm^3 for normal group, which significantly decreased to 700 mg/cm^3 for RA rats. And pure P had no effects on BMD so that the BMD of RA + P group was 706 mg/cm^3. Nevertheless, the BMD became 721 mg/cm^3 and 725 mg/cm^3 for RA + DP-M$_{(H)}$ and RA + DP-B$_{(H)}$ groups respectively. The DPs could effectively improve the BMD of RA rats. Furthermore, the body weight was also a useful judgement of therapeutic effects. As shown in Fig. 6F, the body weight maintained slightly increasing from 218 to 230 g versus time for normal group while it significantly went down below 200 g since day 21. Conversely, the body weight did not decrease and maintained around 209–211 g for RA + P group. However, DPs obviously increased the body weight, close to that of normal group since day 21.

The inflammatory level of serum was also evaluated by ELISA. As shown in i of Fig. 6G, the gene expression of IL-6 was 269.8 for normal rats while it significantly increased to 361.9 for RA group and 330.9 for RA + P group respectively. After the treatment of DPs, the gene expression sharply decreased to 322.2 for RA + DP-M$_{(H)}$ group and 300.9 for RA + DP-B$_{(H)}$ group. The similar trend was also observed for the expression of MMP-13, TNF-α and IL-1β (ii, iii and iv of Fig. 6G). In the meantime, high local cfDNA concentration was detected for RA group (Fig. 6H), confirming that cfDNA could act as a biomarker in RA. The concentration of cfDNA from serum in normal group was 9 μg/mL, sharply increased to 52 μg/mL for RA group while it became 33 μg/mL after P treatment. Significantly, the concentration of cfDNA was 24 μg/mL for RA + DP-M$_{(H)}$ group and 13 μg/mL for RA + DP-B$_{(H)}$ group respectively. Besides, the expression levels of IL-6, MMP-13 and TNF-α for SF were also investigated by ELISA. All inflammatory factors significantly increased for RA group compared to normal group. And it was observed that P could decrease the expression of inflammatory factors to a certain extent. However, DPs obviously reduced their expression levels, especially for DP-B$_{(H)}$ with the expression levels close

to normal group (Fig. 6I).

The bone erosion caused by synovial cavity inflammation became worse and worse during the progression of RA. The histological results of knee joints were illustrated in Fig. 7. As shown in H&E (Fig. 7A) and Safranin O (Fig. 7B) images, the RA + P and RA + DP-M$_{(H)}$ groups presented various proteoglycan retention degrees, bone erosion attenuation, and tidemark integrity promotion, while these characteristics were deterioration over time in RA group. Although RA + P and RA + DP-M$_{(H)}$ groups exhibited potential of cartilage repair, their performances were still far away from DP-B$_{(H)}$ group with significantly reduced synovial hyperplasia and cartilage destruction, which was close to the normal knee joints. Besides, DPs inhibited the inflammation in CIA rats as the significantly decreased expression of IL-6, MMP-13 and TNF-α. From Fig. 7C, the immunohistochemical staining also confirmed the above results, as the protein expression of IL-6, TNF-α and MMP-13 in cartilage was significantly inhibited by DP-B$_{(H)}$ treatment, which was evidenced by light and sparsely dying of these markers. However, the positive staining (dark brown) of these proteins was significantly observed on the cartilage surface for RA group and it slightly became light for RA + P group. In the meantime, although apparently decreased expression of IL-6 and TNF-α was observed for RA + DP-M$_{(H)}$ group, its expression of MMP-13 still maintained a certain level, not better than that of RA + DP-B$_{(H)}$ group. Thus, DPs inhibited the progression of RA, especially for DP-B$_{(H)}$, with highest charge density among them, exhibited an outstanding scavenging of cfDNA owing to the high affinity of cfDNA binding, which endowed it with superior anti-inflammatory and excellent effects of RA therapy.

In the meantime, the histological results of ankle joints were also investigated to evaluate the RA therapy effects (Fig. S11). Similar to knee joints, the obvious hyperplasia and cartilage destruction were observed for the ankle joints of RA group while they almost maintained the same conditions for RA + P group. However, the alleviated hyperplasia and cartilage destruction significantly occurred for RA + DP-M$_{(H)}$ and RA + DP-B$_{(H)}$ groups. Specifically for RA + DP-B$_{(H)}$ group, the apparent repaired effects were observed, infinitely close to normal group. In addition, the potential *in vivo* cytotoxicity of PDA NPs was still evaluated for biosafety concerns. The histological analysis was applied to investigate *in vivo* cytotoxicity after RA treatment for 2 weeks. As shown in Fig. S12, the major organs including heart, liver, spleen, lung and kidney maintained the normal state, and no obvious damaged tissue or inflammatory lesions were observed for all groups, indicating that these treatment strategies could act as an excellent RA therapy with minimal cytotoxicity. Previous study of a novel polyamidoamine dendrimer (PAMAM) had discovered the potential advantages of nucleic acid scavenger on mitigation of pro-inflammatory effects [49]. Furthermore, a highly cationic surface caused by methylation of the primary amines increased DNA scavenging and significantly reduced inflammatory responses induced by CpG [50]. And inflammatory factors, such as MMP-3 was a protease produced by synovial tissues and played the important roles in the progression of joint destruction [51]. Thus, the reduction of MMP-3 was a pleasurable marker for RA treatment.

Therefore, PDA NPs with huge amount of reductant groups could attenuated cartilage damage and synovial hyperplasia, exhibiting chondro-protection in CIA rats, which provided anatomical structure for functional recovery. Significantly, DPs, especially DP-B$_{(H)}$, with high cfDNA binding affinity due to its high positive charge density, another reason for exhibiting the excellent effects of RA therapy. Besides, the negatively charged surface in cartilage also contributed to the high efficacy of RA therapy by cationic scavengers. Containing negative glycosaminoglycans (GAGs), cartilage provided binding affinity sites for the cationic agents, which facilitated the uptake of arthritis drugs and prolonged their retention time [52,53].
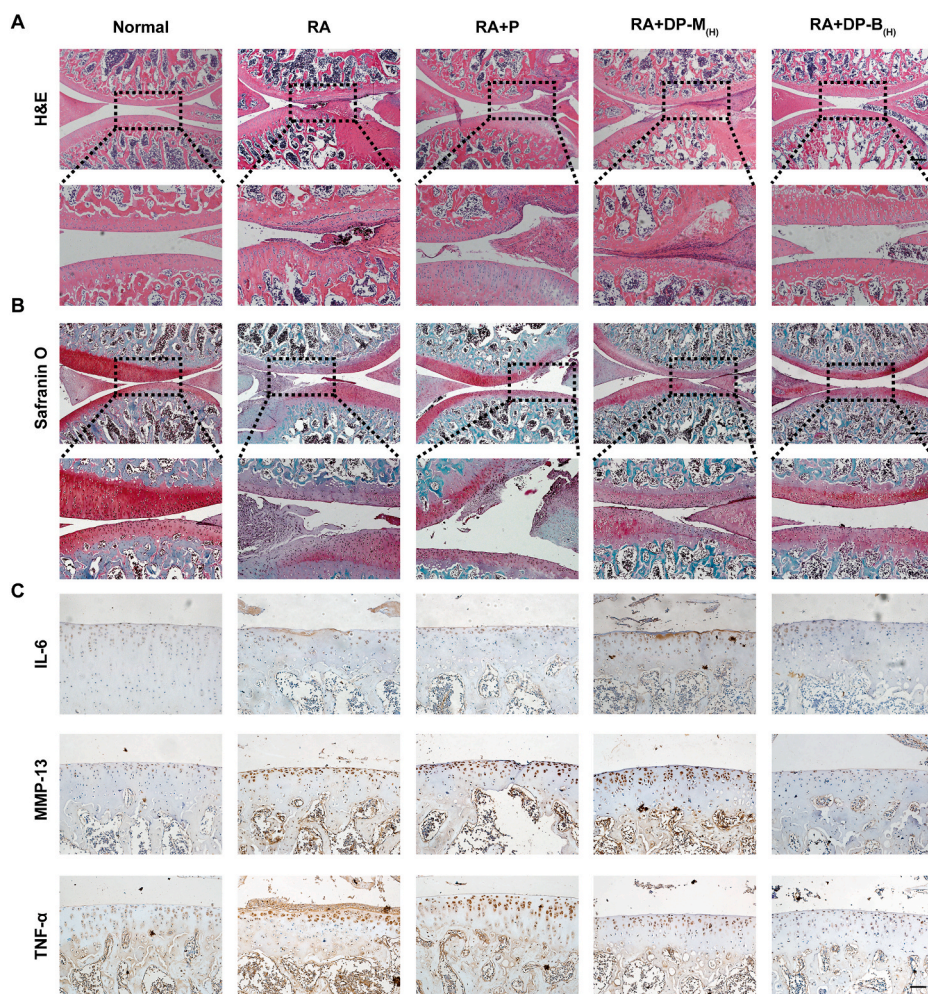
Fig. 7. Histological results of *in vivo* therapeutic effects. A) Representative images of H&E staining on knee joints. B) Representative images of Safranin O staining on knee joints. C) Representative images of immunohistochemical staining (IL-6, MMP-3 and TNF-α) on knee joints. The corresponding groups respectively were: normal (normal rats), RA (CIA rats), RA + P (CIA rats followed by P treatment), RA + DP-M(H) (CIA rats followed by DP-M(H) treatment), RA + DP-B(H) (CIA rats followed by DP-B(H) treatment). (Bar = 100 μm).

4. Conclusions

To avoid the intrinsic cytotoxicity of positively charged cfDNA scavengers and maintain their inhibitory function is important for designing therapeutic agents for RA therapy. Herein, P was modified by M or B with different amount, forming DPs including DP-M(L), DP-M(H), DP-B(L) and DP-B(H) with different positive charge density. The DPs have superior binding affinity of cfDNA and little cytotoxicity, which effectively inhibited LPS induced inflammation *in vitro*, resulting in the relief of joint swelling, synovial hyperplasia and cartilage destruction in RA rats. Particularly, DP-B(H) with high DS of bis dimethylamino groups exhibited superior cfDNA binding affinity, leading to the best therapeutic effects among all groups. These findings suggested the novel DP NPs could act as potential agents for RA therapy, which was conducive to design the safe and effective DNA scavengers for other cfDNA related diseases.

CRediT authorship contribution statement

Ying Chen: participated in the, Investigation, data processing and, Formal analysis, experiment management, participated in the data processing and, Formal analysis, participated in revising the manuscript. **Yonglin Wang:** participated in the, Investigation, data processing and, Formal analysis, experiment management, participated in the data processing and, Formal analysis. **Xianfang Jiang:** participated in the paper writing, participated in the data processing and, Formal analysis. **Jinhong Cai:** participated in the, Investigation, data processing and, Formal analysis, experiment management, participated in the data processing and, Formal analysis, participated in revising the manuscript. **Yuting Chen:** participated in revising the manuscript, All authors have read and agreed to the published version of the paper. **Hanji Huang:** participated in revising the manuscript. **Yuan Yang:** participated in revising the manuscript. **Li Zheng:** participated in the paper writing, acquired the, Funding acquisition, participated in the study conception, Data curation, Formal analysis, and, Writing – review & editing, and finalized this paper. **Jinmin Zhao:** acquired the, Funding acquisition, participated in the study conception, Data curation, Formal analysis, and, Writing – review & editing, and finalized this paper. **Ming Gao:** participated in the paper, Writing – original draft, participated in the data processing and, Formal analysis, participated in revising the manuscript, corresponding authors, participated in revising the manuscript, acquired the, Funding acquisition, participated in the study conception, Data curation, Formal analysis, and, Writing – review & editing, and finalized this paper.

Declaration of competing interest

No potential conflicts of interest were disclosed.

Acknowledgments

GuikeAD19254003).

Appendix A. Supplementary data

Supplementary data to this article can be found online at https://doi.org/10.1016/j.bioactmat.2022.03.028.

References

[1] M. Snyder, M. Kircher, A. Hill, R. Daza, J. Shendure, Cell-free DNA comprises an InVivo nucleosome footprint that informs its tissues-of-origin, Cell 164 (2016) 57–68.
[2] E. Heitzer, L. Auinger, M.R. Speicher, Cell-free DNA and apoptosis: how dead cells inform about the living, Trends Mol. Med. 26 (2020) 519–528.
[3] D. Han, Y. Lo, The nexus of cfDNA and nuclease biology, Trends Genet. 37 (2021) 758–770.
[4] T. Hasimoto, K. Yoshida, N. Hashimoto, K. Kaneshiro, A. Nakai, Y. Kawasaki, A. Hashiramoto, AB0248 circulating cell free DNA; A marker to predict the therapeutic response for biological dmards in rheumatoid arthritis, Ann. Rheum. Dis. 75 (2016) 983.1-983.
[5] A. Antonyan, R. Harutyunyan, S. Sharoyan, L. Karapetyan, S. Mardanyan, AB0032The adenosine deaminase isoforms activity in synovial fluid in patients with different arthritis, Ann. Rheum. Dis. 75 (2016) 907.3-908.
[6] C. Dong, Y. Liu, C. Sun, H. Liang, L. Liu, Identification of specific joint-inflammatogenic cell-free DNA molecules from synovial fluids of patients with rheumatoid arthritis, Front. Immunol. 11 (2020) 662.
[7] D.N. Daraghmeh, C. King, M.D. Wiese, A review of liquid biopsy as a tool to assess epigenetic, cfDNA and miRNA variability as methotrexate response predictors in patients with rheumatoid arthritis, Pharmacol. Res. 173 (2021), 105887.
[8] P. Mondelo-Macia, P. Castro-Santos, A. Castillo-Garcia, L. Muinelo-Romay, R. Diaz-Pena, Circulating free DNA and its emerging role in autoimmune diseases, J. Personalized Med. 11 (2021) 1–14.
[9] H. Liang, B. Peng, C. Dong, L. Liu, J. Mao, S. Wei, X. Wang, H. Xu, J. Shen, H.Q. Mao, Cationic nanoparticle as an inhibitor of cell-free DNA-induced inflammation, Nat. Commun. 9 (2018) 4291.
[10] G. Chamilos, J. Gregorio, S. Meller, R. Lande, D.P. Kontoyiannis, R.L. Modlin, M. Gilliet, Cytosolic sensing of extracellular self-DNA transported into monocytes by the antimicrobial peptide LL37, Blood 120 (2012) 3699.
[11] J. Tian, A.M. Avalos, S.Y. Mao, B. Chen, K. Senthil, H. Wu, P. Parroche, S. Drabic, D. Golenbock, C. Sirois, Toll-like receptor 9-dependent activation by DNA-containing immune complexes is mediated by HMGB1 and RAGE, Nat. Immunol. 8 (2007) 487–496.
[12] H. Yang, H. Wang, U. Andersson, Targeting inflammation driven by HMGB1, Front. Immunol. 11 (2020) 484.
[13] Y. Yan, H. Liang, X. Liu, L. Liu, Y. Chen, Topical cationic hairy particles targeting cell free DNA in dermis enhance treatment of psoriasis, Biomaterials 276 (2021) 121027.
[14] S. Temburni, R.M. Andersen, S.L. Allen, J.C. Barrientos, R.N. Damle, TLR-9 and B-cell antigen receptor triggering of primary B cells from mantle cell lymphoma induce cell proliferation and telomerase activity, Blood 118 (2011) 3690.
[15] K. Svetlana, S. Tatiana, K. Larisa, P. Lev, S. Anatolij, E. Elizaveta, S. Sergey, I. Vera, V. Natalia, GC-rich extracellular DNA induces oxidative stress, double-strand DNA breaks, and DNA damage response in human adipose-derived mesenchymal stem cells, 2015, Oxid. Med. Cell. Longev. (2015), 782123.
[16] M. Rodero, A. Tesser, E. Bartok, G. Rice, E.D. Mina, Type I interferon-mediated autoinflammation due to DNase II deficiency, Nat. Commun. 8 (2017) 2176.
[17] S. Pawaria, K. Nündel, K. Gao, S. Moses, P. Busto, K. Holt, Role of interferon-γ–producing Th1 cells in a murine model of type I interferon–independent autoinflammation resulting from DNase II deficiency, Arthritis Rheumatol. 72 (2020).
[18] H. Kilpinen, S. Waszak, A. Gschwind, S. Raghav, R. Witwicki, Coordinated effects of sequence variation on DNA binding, chromatin structure, and transcription, Science (New York, N.Y.) 342 (2013) 744–747.
[19] U. LaChelt, E. Wagner, Nucleic acid therapeutics using polyplexes: a journey of 50 Years (and beyond), Chem. Rev. 115 (2015) 11043–11078.
[20] J. Dawulieti, M. Sun, Y. Zhao, D. Shao, H. Yan, Treatment of severe sepsis with nanoparticulate cell-free DNA scavengers, Adv. Sci. 6 (2020), eaay7148.
[21] Y.L. Yun, H.H. Park, W. Park, H. Kim, C.G. Park, Long-acting nanoparticulate DNase-1 for effective suppression of SARS-CoV-2-mediated neutrophil activities and cytokine storm, Biomaterials 267 (2021), 120389.
[22] Q. Zhang, D. Dehaini, Y. Zhang, J. Zhou, X. Chen, L. Zhang, R.H. Fang, W. Gao, L. Zhang, Neutrophil membrane-coated nanoparticles inhibit synovial inflammation and alleviate joint damage in inflammatory arthritis, Nat. Nanotechnol. 13 (2018) 1182–1190.
[23] X. Liu, J. Cao, H. Li, J. Li, Q. Jin, K. Ren, J. Ji, Mussel-Inspired polydopamine: a biocompatible and ultrastable coating for nanoparticles in vivo, ACS Nano 7 (2013) 9384–9395.
[24] T. Zhou, L. Yan, C. Xie, P. Li, L. Jiang, J. Fang, C. Zhao, F. Ren, K. Wang, Y. Wang, H. Zhang, T. Guo, X. Lu, A mussel-inspired persistent ROS-scavenging, electroactive, and osteoinductive scaffold based on electrochemical-driven in situ nanoassembly, Small 15 (2019), 1805440.

[25] X. Bao, J. Zhao, S. Jian, M. Hu, X. Yang, Polydopamine nanoparticles as efficient scavengers for reactive oxygen species in periodontal disease, ACS Nano 12 (2018) 8882–8892.
[26] B.V. Long, Y. Sato, P. Chonpathompikunlert, S. Tanasawet, Y. Nagasaki, Self-assembled polydopamine nanoparticles improve treatment in Parkinson's disease model mice and suppress dopamine-induced dyskinesia, Acta Biomater. 109 (2020) 220–228.
[27] X. Wang, H. Zhao, Z. Liu, Y. Wang, S.G. Shen, Polydopamine nanoparticles as dual-task platform for osteoarthritis therapy: a scavenger for reactive oxygen species and regulator for cellular powerhouses, Chem. Eng. J. 417 (2021), 129284.
[28] J. Li, W. Hou, S. Lin, L. Wang, C. Pan, F. Wu, J. Liu, Polydopamine nanoparticle-mediated dopaminergic immunoregulation in colitis, Adv. Sci. (2021), e2104006.
[29] H.J. Cha, S.H. Dong, S. Lim, Development of bioadhesives from marine mussels, Biotechnol. J. 3 (2008) 631–638.
[30] Y. Meng, P. Liu, W. Zhou, J. Ding, J. Wen, Bioorthogonal DNA adsorption on polydopamine nanoparticles mediated by metal coordination for highly robust sensing in serum and living cells, ACS Nano 12 (2018) 9070–9080.
[31] Y. Liu, K. Ai, L. Lu, Polydopamine and its derivative materials: synthesis and promising applications in energy, environmental, and biomedical fields, Chem. Rev. 114 (2014) 5057–5115.
[32] Z. Zhu, P. Wu, G. Liu, X. He, B. Qi, G. Zeng, W. Wang, Y. Sun, F. Cui, Ultrahigh adsorption capacity of anionic dyes with sharp selectivity through the cationic charged hybrid nanofibrous membranes, Chem. Eng. J. 313 (2016) 957–966.
[33] Y. Wang, X. Ma, C. Ding, L. Jia, pH-responsive deoxyribonucleic acid capture/release by polydopamine functionalized magnetic nanoparticles - ScienceDirect, Anal. Chim. Acta 862 (2015) 33–40.
[34] A. Priyam, P. Nagar, A.K. Sharma, P. Kumar, Mussel-inspired polydopamine-polyethylenimine conjugated nanoparticles as efficient gene delivery vectors for mammalian cells, Colloids Surf. B Biointerfaces 161 (2018) 403–412.
[35] I. Zmerli, J.P. Michel, A. Makky, Bioinspired polydopamine nanoparticles: synthesis, nanomechanical properties, and efficient PEGylation strategy, J. Mater. Chem. B 8 (2020) 4489–4504.
[36] E. Pretorius, O.O. Akeredolu, P. Soma, D.B. Kell, Major involvement of bacterial components in rheumatoid arthritis and its accompanying oxidative stress, systemic inflammation and hypercoagulability, Exp. Biol. Med. 242 (2017) 355–373.
[37] P. Mark, A. Sharareh, Z.A. Claudia, Cell-free DNA release by mouse placental explants, PLoS One 12 (2017), e0178845.
[38] J. Wang, Y. Wang, H. Zhang, J. Chang, Z. Yin, Identification of a novel microRNA-141-3p/Forkhead box C1/β-catenin axis associated with rheumatoid arthritis synovial fibroblast function in vivo and in vitro, Theranostics 10 (2020) 5412–5434.
[39] J. Wu, H. Liang, Y. Li, Y. Shi, M. Bottini, Y. Chen, L. Liu, Cationic block copolymer nanoparticles with tunable DNA affinity for treating rheumatoid arthritis, Adv. Funct. Mater. 30 (2020), 2000391.
[40] Y. Yan, H. Liang, X. Liu, L. Liu, Y. Chen, Topical cationic hairy particles targeting cell free DNA in dermis enhance treatment of psoriasis, Biomaterials 276 (2012) 121027.
[41] S. Xue, X. Zhou, W. Sang, C. Wang, H. Lu, Y. Xu, Y. Zhong, L. Zhu, C. He, J. Ma, Cartilage-targeting peptide-modified dual-drug delivery nanoplatform with NIR laser response for osteoarthritis therapy, Bioact Mater 6 (2021) 18.
[42] J. Wu, H. Liang, Y. Li, Y. Shi, M. Bottini, Y. Chen, L. Liu, Cationic block copolymer nanoparticles with tunable DNA affinity for treating rheumatoid arthritis, Adv. Funct. Mater. 30 (2020), 2000391.
[43] C. Ma, B. Li, J. Zhang, Y. Sun, J. Li, H. Zhou, J. Shen, R. Gu, J. Qian, C. Fan, H. Zhang, K. Liu, Significantly improving the bioefficacy for rheumatoid arthritis with supramolecular nanoformulations, Adv. Mater. 33 (2021), e2100098.
[44] H. Liang, Y. Yan, J. Wu, X. Ge, Y. Chen, Topical nanoparticles interfering with the DNA-LL37 complex to alleviate psoriatic inflammation in mice and monkeys, Sci. Adv. 6 (2020), eabb5274.
[45] B. Yang, H. Yao, J. Yang, C. Chen, Y. Guo, H. Fu, J. Shi, In Situ Synthesis of Natural Antioxidase Mimics for Catalytic Anti-inflammatory Treatments: Rheumatoid Arthritis as an Example, J Am Chem Soc, 2021.
[46] H. Tsuchiya, M. Ota, K. Fujio, Multiomics landscape of synovial fibroblasts in rheumatoid arthritis, Inflamm. Regen. 41 (2021) 7.
[47] H. Tsuchiya, M. Ota, S. Sumitomo, K. Ishigaki, K. Fujio, Parsing multiomics landscape of activated synovial fibroblasts highlights drug targets linked to genetic risk of rheumatoid arthritis, Ann. Rheum. Dis. 80 (2020) annrheumdis-2020-218189.
[48] K.W. Kim, B.M. Kim, J.Y. Won, H.K. Min, K.A. Lee, S.H. Lee, H.R. Kim, Regulation of osteoclastogenesis by mast cell in rheumatoid arthritis, Arthritis Res. Ther. 23 (2021) 124.
[49] S.C. Hyde, I.A. Pringle, S. Abdullah, A.E. Lawton, L.A. Davies, A. Varathalingam, G. Nunez-Alonso, A.M. Green, R.P. Bazzani, S.G. Sumner-Jones, CpG-free plasmids confer reduced inflammation and sustained pulmonary gene expression, Nat. Biotechnol. 26 (2008) 549–551.
[50] J. Lee, J.G. Jackman, J. Kwun, M. Manook, A. Moreno, E.A. Elster, A. Kirk, K.W. Leong, B.A. Sullenger, Nucleic acid scavenging microfiber mesh inhibits trauma-induced inflammation and thrombosis, Biomaterials 120 (2017) 94–102.
[51] J. Jing, J.D. Ma, Y.Q. Mo, L.F. Chen, L. Dai, AB0216Overexpression of synovial lining peroxisome proliferator-activated receptor-gamma coactivator-1β involved

in joint destruction through upregulating MMP-3 in rheumatoid arthritis, Ann. Rheum. Dis. 75 (2016), 971.2-972.

[52] A.G. Bajpayee, A.J. Grodzinsky, Cartilage-targeting drug delivery: can electrostatic interactions help? Nat. Rev. Rheumatol. 13 (2017) 183–193.

[53] A. Av, A. Ekw, A. Sm, A. Th, A. Cz, B. Agba, Cartilage penetrating cationic peptide carriers for applications in drug delivery to avascular negatively charged tissues, Acta Biomater. 93 (2019) 258–269.